SCIENCE CHINA
Earth Sciences

• RESEARCH PAPER •

December 2010 Vol.53 Suppl. I: 26–33
doi: 10.1007/s11430-010-4127-4

Quantitative estimation of the shrub canopy *LAI* from atmosphere-corrected HJ-1 CCD data in Mu Us Sandland

CHEN Wei[1,2], CAO ChunXiang[1*], HE QiSheng[1,2], GUO HuaDong[3], ZHANG Hao[1,2], LI RenQiang[4], ZHENG Sheng[1,2], XU Min[1,2], GAO MengXu[1,2], ZHAO Jian[1,2], LI Sha[1], NI XiLiang[1,2], JIA HuiCong[1], JI Wei[1], TIAN Rong[1,2], LIU Cheng[1,2], ZHAO YuXing[5] & LI JingLu[6]

[1] *State Key Laboratory of Remote Sensing Science, Jointly Sponsored by the Institute of Remote Sensing Applications of Chinese Academy of Sciences and Beijing Normal University, Beijing 100101, China;*
[2] *Graduate University of Chinese Academy of Sciences, Beijing 100049, China;*
[3] *Center for Earth Observation and Digital Earth, Chinese Academy of Sciences, Beijing 100190, China;*
[4] *China Key Laboratory of Ecological Network Observation and Modeling, Institute of Geographical Sciences and Natural Resources Research, Chinese Academy of Sciences, Beijing 100101, China;*
[5] *Ordos Forestry Sand Control Science Institute, Dongsheng 017000, China;*
[6] *Inner Mongolia Biomass Thermoelectricity Limited Company, Wushen 017300, China*

Received March 31, 2010; accepted November 10, 2010

The leaf area index (*LAI*) is an important ecological parameter that characterizes the interface between vegetation canopy and the atmosphere. In addition, it is used by most process-oriented ecosystem models. This paper investigates the potential of HJ-1 CCD data combined with linear spectral unmixing and an inverted geometric-optical model for the retrieval of the shrub *LAI* in Wushen Banner of Inner Mongolia in the Mu Us Sandland. MODTRAN (Moderate Resolution Atmospheric Radiance and Transmittance Model) was used for atmospheric correction. Shrubland was extracted using the threshold of the normalized difference vegetation index, with which water bodies and farmland were separated, in combination with a vegetation map of the People's Republic of China (1:1000000). Using the geometric-optical model, we derive the per-pixel reflectance as a simple linear combination of two components, namely sunlit background and other. The fraction of sunlit background is related to the shrub *LAI*. With the support of HJ-1 CCD data, we employ linear spectral unmixing to obtain the fraction of sunlit background in an atmospherically corrected HJ image. In addition, we use the measured shrub canopy structural parameters for shrub communities to invert the geometric-optical model and retrieve the pixel-based shrub *LAI*. In total, 18 sample plots collected in Wushen Banner of Inner Mongolia are used for validation. The results of the shrub *LAI* show good agreement with R^2 of 0.817 and a root-mean-squared error of 0.173.

shrub leaf area index inversion, HJ-1 data, geometric-optical model, MODTRAN, Mu Us Sandland

Citation: Chen W, Cao C X, He Q S, et al. Quantitative estimation of the shrub canopy *LAI* from atmosphere-corrected HJ-1 CCD data in Mu Us Sandland. Sci China Earth Sci, 2010, 53(Suppl. I): 26−33, doi: 10.1007/s11430-010-4127-4

The leaf area is the main surface of energy and matter exchange between the plant canopy and atmosphere, and therefore an important variable in driving the biological processes of plants. The leaf area index (*LAI*), defined [1] as half the total leaf area per unit ground surface area, is also a useful ''bulk'' parameter and a necessary input parameter in

*Corresponding author (email: cao413@irsa.ac.cn)

many models. The *LAI* characterizes the canopy-atmosphere interface of an ecosystem, and is therefore related to precipitation and atmospheric nutrient deposition interception, canopy microclimate, radiation extinction, and water, carbon, and energy exchanges with the atmosphere. For parameterization of the land-type distribution, the *LAI* has traditionally been mapped from remote sensing imagery with different resolutions [2–11].

In arid environments with very low leaf area per unit area, the main physical phenomenon underlying observed changes is shadowing of the background by plants. Models that exp*LAI*n changes in the spectral reflectance of a partly vegetated surface with respect to illumination and viewing angle and the physical structure and optical properties of canopy elements have been developed. These models attempt to describe and may partly exp*LAI*n the surface bidirectional reflectance distribution function (BRDF). Geometric-optical (GO) models are one class of such models and they treat the surface as an assemblage of discrete, identical, and relatively large geometric objects having a Poisson distribution above an underlying surface [12, 13] that is frequently considered Lambertian but may also be characterized by its own BRDF [14]. The remote-sensing observation is modeled as a linear combination of contributions from viewed sunlit and shaded components, with each contribution a product of component reflectance and the fraction of the sensor's field of view occupied by the component [14].

GO models have been used to estimate forest canopy metrics and appear to have great potential [16, 17]. The Li-Strahler GO model [10] is one of the best known of this type of model and has been found to perform well for forest environments. Similar models have also been used in theoretical and validation studies of desert grasslands and shrublands [18–20]. In spite of their successful application for forests, GO models have been less used in estimating shrub canopy parameters for drylands at landscape scales [15]. This may be because the background of forest environments makes a small contribution to the signal relative to tree crowns and is often composed of a fairly homogeneous understory with relatively high coverage and spectral reflectance characteristics similar to those of tree leaves and dark organic soils. Several workers have noted that, even in forest environments, the understory can present problems in GO modeling [21, 22]. The background of mineral soils, litter and mixed understory plant cover of grasses, subshrubs and annuals governs brightness much more in arid environments than in forests. Background (soil plus understory) fractional cover usually exceeds 0.7 and the high brightness relative to leaves, stalks and branches of large plants reduces the vegetation-specific information content of the signal [14]. In this paper, a GO model is used for shrub *LAI* inversion.

The Environment and Disaster Monitoring and Forecasting by Small Satellite Constellation A and B satellites (HJ-1A/B satellites) were launched on September 6, 2008. There have been few studies on the application of HJ-1 satellite data [23, 24]. Ecology environmental parameter inversion should be strengthened to extend its application.

Our study estimates the shrub *LAI* from HJ-1 data using the GO model. Firstly, the Moderate Resolution Atmospheric Radiance and Transmittance Model (MODTRAN) model was used for atmospheric correction of HJ-1 data. Secondly, shrubland was extracted using a normalized difference vegetation index (NDVI) threshold in combination with a vegetation map of the People's Republic of China (1:1000000). The inverted GO model combined with spectral unmixing analysis was then employed to extract the shrub *LAI*. Finally, the inversion result obtained from the GO model was validated.

1 Study area and data

The Mu Us Sandland is located at the junction of Ningxia, Inner Mongolia and Shanxi province with geographic coordinates ranging from 37°29′N to 39°20′N in latitude and from 107°20′E to 110°30′E in longitude. The region includes the southern city of Ordos in Inner Mongolia, the northern part of Shaanxi Yulin and the north-east part of the Ningxia Hui Autonomous Region. The Mu Us Sandland, with an area of about 4×10^4 km^2, is in the transition between the Ordos Plateau and the Loess Plateau, and the region has a continental semi-arid climate. Our study area ranging from 37°39′N to 39°24′N in latitude and from 108°17′E to 109°40′E in longitude is located in the hinterland of the Mu Us Sandland in Wushen Banner, Ordos City, Inner Mongolia Autonomous Region (Figure 1). This area has an extreme temperate continental climate with low rainfall, droughts, strong winds and evaporation and abundant sunshine; annual precipitation is 350 to 400 mm, annual evaporation is about 2592 mm, the annual average temperature is 6 to 8°C, the annual average of sunshine hours are 2860 h, the annual average accumulated temperature is 2621°C, the annual average wind speed is 3.4 m s^{-1}, and the average number of days on which the wind is gale 8 or above is more than 24. Wind-blown sand accounts for 78.3% of the total area of Wushen Banner, which also includes meadow soil, chestnut soil, saline soil, loess soil, and swamp soil [25]. Shrubs in the Mu Us Sandland mainly comprise Tamarix, Salix psammophila, Hippophae rhamnoides, Peking willow, Caragana, scoparium, Artemisia, Hedysarum, and Salix cheilophila.

The Environment and Disaster Monitoring and Forecasting by Small Satellite Constellation A and B satellites (HJ-1A/B satellites) were launched at 11:25 on September 6, 2008. The HJ-1A satellite is equipped with a charge- coupled device (CCD) camera and a hyperspectral image radiometer (HSI), and the HJ-1B satellite is equipped with a CCD camera and infrared camera (IRS). The CCD cameras of the HJ-1A and HJ-1B satellite are of the same design,

having nadir symmetrical placement and split fields and making parallel observations. They are combined to achieve four-spectrum pushbroom imaging with a ground swath width of 700 km and ground pixel resolution of 30 m. In addition, the HJ-1A satellite is equipped with an HSI to achieve 110–128-spectrum pushbroom imaging with a ground swath width of 50 km and ground pixel resolution of 100 m. The HSI has a ±30° side view and onboard calibration capabilities. The HJ-1B satellite is loaded with an IRS to achieve imaging with a ground swath width of 720 km and ground pixel resolution of 150 or 300 m for the near-infrared, mid-infrared and infrared. The main parameters are listed in Table 1.

In this paper, the HJ-1B CCD2 image acquired on 2 July 2009 was used for analysis. Meanwhile, the land-use and land-cover map for the year 2000 and a vegetation map of the People's Republic of China (1:1000000) were used for shrub extraction. Because the region has been little affected by humans, the map is useful for shrub extraction. The capability of using HJ-1 satellite data to extract the shrub *LAI* was investigated through field work from 3 to 15 July 2009. The location of each sample site was fixed using a global positioning system (GPS) with an error of 6 m. At each site, the *LAI* was measured using an *LAI*2000 device. As the spatial resolution of the HJ-1B CCD image is 30 m, to match the *in situ* observed *LAI* to the pixel *LAI* value retrieved from remote sensing, we measured the *LAI* in each 30 m × 30 m plot, and the final *LAI* was taken as the average value of nine points distributed evenly in the sample space.

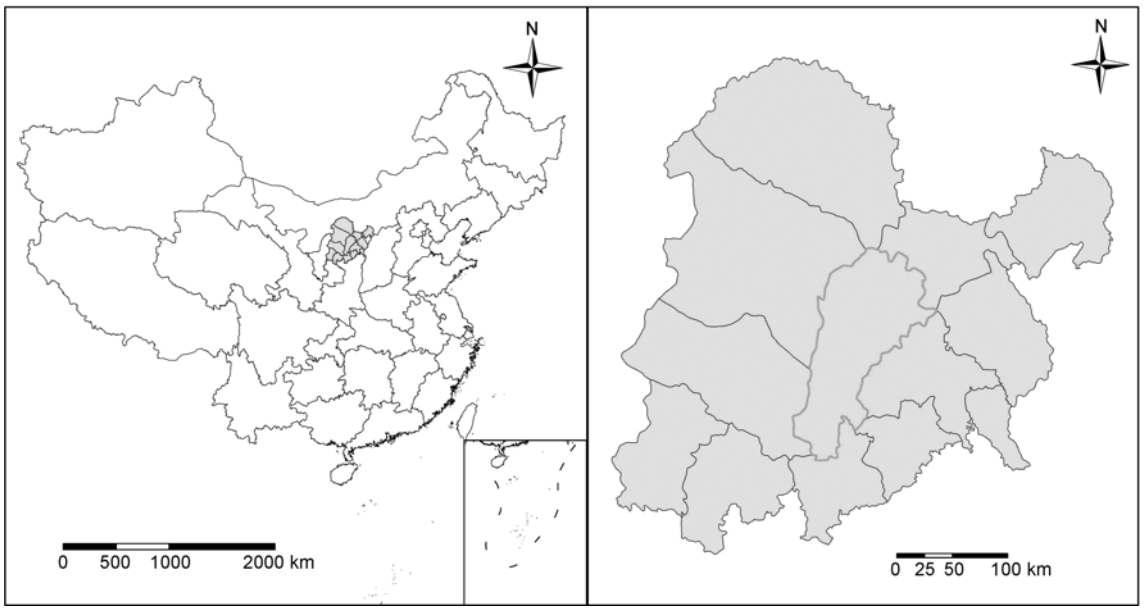

Figure 1 Location of the study area. (a) Location of the Mu Us Sandland in China; (b) a magnified map of the indicated area showing the location of Wushen Banner.

Table 1 Characteristics of the HJ-1A/B satellites

Satellite	Sensor	Band	Wavelength range (μm)	Spatial resolution (m)	Swath width (km)	Sub-cycle (day)
HJ-1A	CCD	1	0.43–0.52	30	360	4
		2	0.52–0.60	30		
		3	0.63–0.69	30		
		4	0.76–0.90	30		
	HSI	–	0.45–0.95	100	50	4
HJ-1B	CCD	1	0.43–0.52	30	360	4
		2	0.52–0.60	30		
		3	0.63–0.69	30		
		4	0.76–0.90	30		
	IRS	5	0.75–1.10	150	720	4
		6	1.55–1.75			
		7	3.50–3.90			
		8	10.5–12.5	300		

2 Methods

Figure 2 is a sequence of methods employed in this study. The sequence involves:

(1) HJ-1 data processing, including radiometric, atmospheric and geometric corrections.

(2) Deriving the per-pixel proportions of two scene components (sunlit canopy and sunlit background) by linear spectral unmixing analysis of HJ-1 surface reflectance data.

(3) Employing the NDVI threshold and a vegetation map of the People's Republic of China (1:1000000) to extract the shrub distribution.

(4) Inverting the GO model integrated with the pixel-based sunlit background fraction and shrub structural parameters to estimate the *LAI*.

(5) Quantitatively assessing the accuracy of model retrievals using collected field data.

Therefore, the key to this study is the theory of the GO model.

2.1 Atmospheric correction based on the MODTRAN model

HJ-1B data were firstly geometrically corrected. The calibrated TM image in the study area was used as the base map, and the same point was selected in TM image and HJ-1B image for correction. Typical features such as road intersections recorded with a GPS handset were then used for verification. Finally, the error of geometric correction was controlled within 0.5 pixels, which meets the geometry correction requirement.

We use the following relation to convert the DN value of the raw image to the at-satellite radiance image using absolute calibration coefficients (Table 2).

$$L = \mathrm{DN} / a + L_0, \tag{1}$$

where L is at-satellite radiance, DN is the digital number of the raw image, a is the absolute calibration coefficient of the gain, and L_0 is the offset. The unit of converted radiance is W m^{-2} sr^{-1} μm^{-1}.

We use the following relation to calculate the at-satellite reflectance.

$$\rho_\lambda = \frac{\pi L_\lambda d^2}{ESUN_\lambda \cos\theta_s}, \tag{2}$$

where ρ_λ is the apparent reflectance of band λ, d is the distance of the astronomical unit from the Sun to the Earth, $ESUN_\lambda$ is the solar spectral irradiance of the upper atmosphere in band λ (Table 3), and θ_s is the solar zenith angle. For the acquired image, the solar zenith angle is 21.767°.

Table 2 Absolute radiometric calibration coefficient of HJ-1B CCD2

HJ-1B CCD2	a (DN (W m^{-2} sr^{-1} μm^{-1})$^{-1}$)	L_0 (W m^{-2} sr^{-1} μm^{-1})
Band 1	0.5782	3.4608
Band 2	0.5087	5.8769
Band 3	0.6825	8.0069
Band 4	0.6468	8.8583

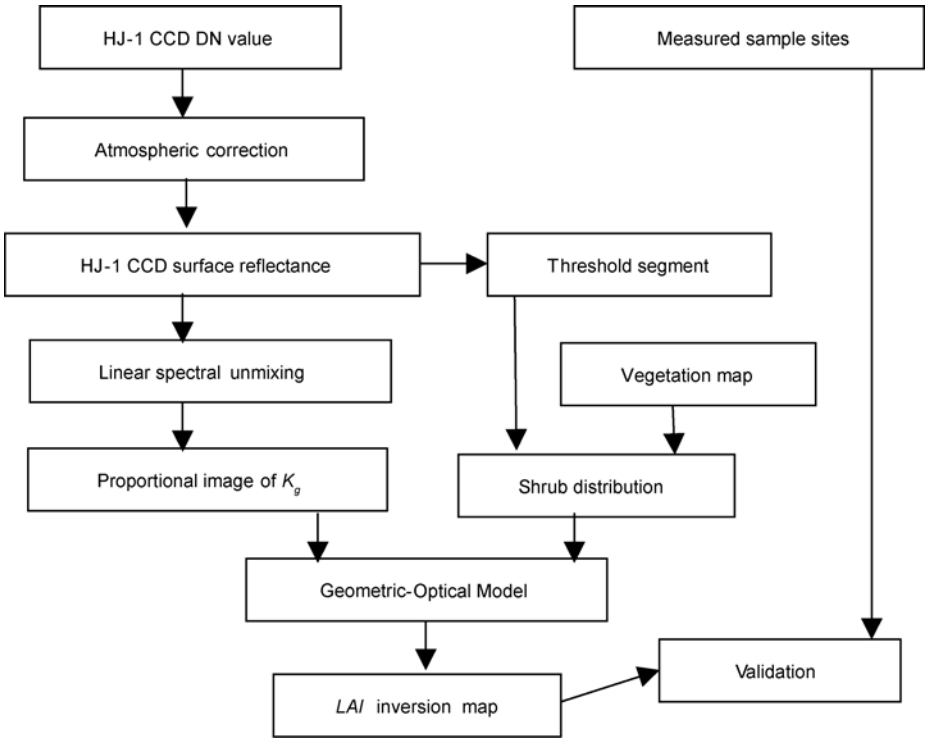

Figure 2 Flow chart of methods employed.

In this paper, MODTRAN was used for atmospheric correction. The MODTRAN model employs a stored spectral database for H_2O, CO_2, O_3, N_2O, CO, CH_4, O_2, NO, SO_2, NO_2, NH_3 and HNO_3. The model includes the effects of scattering (such as Rayleigh and Mie scattering) and allows the user to specify the profiles of temperature, water vapor density, ozone, aerosols and any other gases that may vary with time [26, 27]. In the study area, the aerosol model is of the rural-based aerosol. Aerosol optical thickness is an important parameter for describing aerosol optical properties, and is widely used in radiation transfer and atmospheric correction. However, the visual distance is used as the input parameters in the MODTRAN software. Therefore, the aerosol optical thickness needs to be converted to the visual distance in obtaining the reflectivity.

In MODTRAN, we can calculate the transmittance of the whole layer of the atmosphere and aerosol transmittance when inputting the parameters of the visual distance and selecting the season, the amount of water vapor and other parameters. According to the Lambert-Beer law, we have

$$\tau_a = \int_{z_1}^{z_2} N(z, VIS) \cdot \mathrm{EXT}(\lambda) m_a(z) \mathrm{d}z = -\ln Ta, \quad (3)$$

where $N(z, VIS)$ is the coefficient of aerosol particle density as a function of height (z) and visual distance (VIS), $\mathrm{EXT}(\lambda)$ is an extinction coefficient, λ is the wavelength, $m_a(z)$ is air quality and Ta is aerosol transmittance.

From the different values of VIS and aerosol optical thickness for different seasons, we obtain the relationship between them. In this paper, the relationship between VIS and the aerosol optical thickness in summer at mid-latitude is established (Figure 3). We did not take into account the change in water vapor as it less affected the relationship. Finally, we have

$$\frac{1}{t(550)} = 0.1202V + 0.29735, \quad (4)$$

where $t(550)$ is the aerosol optical thickness at 550 nm and V is the visual distance.

In this paper, the aerosol optical thickness product of MODIS was used for calculating VIS via eq. (4). VIS can then be used as an input parameter in MODTRAN software to obtain the surface reflectivity.

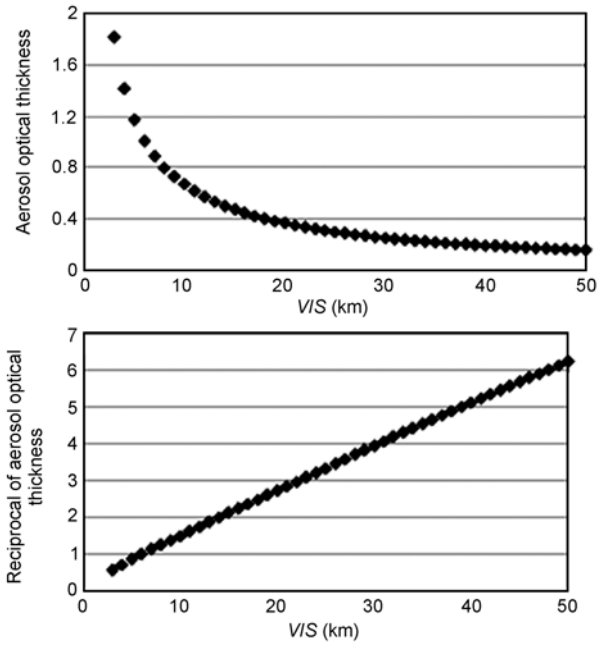

Figure 3 Relationship between VIS and the aerosol optical thickness in summer at mid-latitude. (a) Relationship between VIS and the aerosol optical thickness; (b) relationship between VIS and the reciprocal of aerosol optical thickness.

2.2 GO model

The Li-Strahler GO model [14] was derived from the assumption that the BRDF is a purely geometric phenomenon resulting from a scene of discrete three-dimensional objects being illuminated and viewed from different positions in the hemisphere. The reflectance associated with a given viewpoint is treated as the area-weighted sum of four fixed reflectance components: sunlit canopy (C), shaded canopy (T), sunlit background (G), and shaded background (Z). Therefore, for each pixel of a remote-sensing image, the reflectance (S) can be modeled as a linear combination of four components and their areal proportions (K_g, K_c, K_t and K_z):

$$S = K_g G + K_c C + K_t T + K_z Z. \quad (5)$$

To invert the model, one component (sunlit background) can be used for deriving the expected LAI.

The proportion of sunlit background (K_g) can be formulated using the Boolean model [28]:

$$K_g = \mathrm{e}^{-\pi M\left[\sec(\theta_i)+\sec(\theta_v)-O(\theta_i,\theta_v,\varphi)\right]}. \quad (6)$$

Table 3 Solar irradiance of the upper atmosphere for the CCD camera of the HJ-1A/B satellite (unit: W m^{-2})

	Band 1	Band 2	Band 3	Band 4
HJ-1-A CCD1	1914.324	1825.419	1542.664	1073.826
HJ-1-A CCD2	1929.810	1831.144	1549.824	1078.317
HJ-1-B CCD1	1902.188	1833.626	1566.714	1077.085
HJ-1-B CCD2	1922.897	1823.985	1553.201	1074.544

Here, $O(\theta_i, \theta_v, \phi)$ is the average of the overlap function between illumination and viewing shadows of individual crowns as projected onto the background. ϕ is the difference in azimuth angle between the illumination angle (ϕ_i) and viewing angle (ϕ_v). θ_i and θ_v are the zenith angles of the illumination and observation.

The exact solution for the overlap function on the principal plane is

$$O(\theta_i, \theta_v, \varphi) = 1/\pi\left(\sec\theta_i + \sec\theta_v\right)\left(t - \sin t\cos t\right), \quad (7)$$

where t is given by

$$\cos t = \frac{h\left|\tan\theta_i - \tan\theta_v\cos\varphi\right|}{r\left(\sec\theta_i + \sec\theta_v\right)}. \quad (8)$$

Here, the parameters h and r express the average tree height and the average radius of the crown for the pixel.

From eqs. (6) and (7), M can be inferred as

$$M = \frac{-\ln K_g}{\left(\sec\theta_i + \sec\theta_v\right)\left(\pi - t + \cos t\sin t\right)}. \quad (9)$$

M is an important parameter in the relationship between image variables and vegetation structure. In the case of vegetation with a Poisson distribution, the crown closure is calculated as

$$CC = 1 - \mathrm{e}^{-\pi M}. \quad (10)$$

The canopy gap fraction is a variable that describes the probability of interaction between light and leaves or other canopy components as light travels through the canopy. Thus, the directional canopy gap fraction describes this probability in a specific direction, and it is generally expressed as

$$P(\theta_v, \varphi_v) = \mathrm{e}^{-G(\theta_v,\varphi_v)\Omega LAI/\cos\theta_v}. \quad (11)$$

where θ_v is the viewing zenith angle, φ_v is the viewing azimuth angle, $G(\theta_v, \varphi_v)$ expresses the projected leaf area per unit, LAI is the real leaf area index, and Ω is the clumping index, which is unity when the leaves are randomly distributed [29]. As the clumping situation in the canopy is beyond consideration, the concept of the effective leaf area index LAI_e is employed here. Therefore, eq. (11) can be rewritten as

$$P(\theta_v, \varphi_v) = \mathrm{e}^{-G(\theta_v,\varphi_v)LAI_e/\cos\theta_v}. \quad (12)$$

The crown closure is expressed as

$$CC = 1 - P(\theta_v, \varphi_v), \quad (13)$$

which can be rewritten as

$$1 - CC = \mathrm{e}^{-G(\theta_v,\varphi_v)LAI_e/\cos\theta_v}. \quad (14)$$

We assume that the distribution of the leaf inclination angle of shrubs in the Mu Us Sandland is spherical ($G(\theta_v, \varphi_v)$=0.5), and $\cos\theta_v \approx 1$; eq. (14) can be then be rewritten as

$$1 - CC \approx \mathrm{e}^{-0.5LAI_e}. \quad (15)$$

Transforming eq. (15), the effective LAI and M can be expressed by

$$LAI_e \approx -2\ln(1 - CC) = -2\ln(\mathrm{e}^{-\pi M}) = 2\pi M. \quad (16)$$

2.3 Linear spectral unmixing

Linear spectral unmixing assumes that the reflectance (S) of each pixel is a linear combination of each endmember (E), which is the pure reflectance spectrum of a surface component. The general equations are

$$Sj = \sum_{i=1}^{n} K_i E_{i,j}, \quad (17)$$

$$1 = \sum_{i=1}^{n} K_i, \quad (18)$$

where n is the number of components, j is the band and K is the fractional abundance of an endmember. In this study, eq. (18) is simplified for two fixed reflectance components G and C. The endmembers were selected from the remote-sensing image according to in situ measurements.

3 Results

Firstly, we use the NDVI to extract shrubland from other land types. In this paper, on the basis of NDVI values of main shrubs in the study area obtained from the image, NDVI values from 0.2 to 0.5 were considered representative of shrubs, which easily differentiates shrubland from water bodies, farmland and sand. The land-use and land-cover map and vegetation map of the People's Republic of China (1:1000000) were used to rectify the result by visual interpretation.

The endmembers of sunlit background and other were selected from the HJ-1 data according to *in situ* measurements. Here, we assume $0 \leqslant K_g \leqslant 1$, although a few pixels in the linear spectral unmixing approach produced negative fractions, which subsequently are recoded as infeasible areas with no data in the final mapping results.

Finally, we use the inversion of the GO model integrated with the input data of HJ-1 CCD atmospherically corrected data to derive the LAI distribution. Figure 4 presents the final mapping results of the shrub LAI in Wushen Banner of Inner Mongolia in the Mu Us Sandland.

To validate the model outputs, we use the corresponding inversion value for comparison according to the GPS position. Figure 5 illustrates the agreement between the model-interpreted LAI and ground-measured LAI values. In addi-

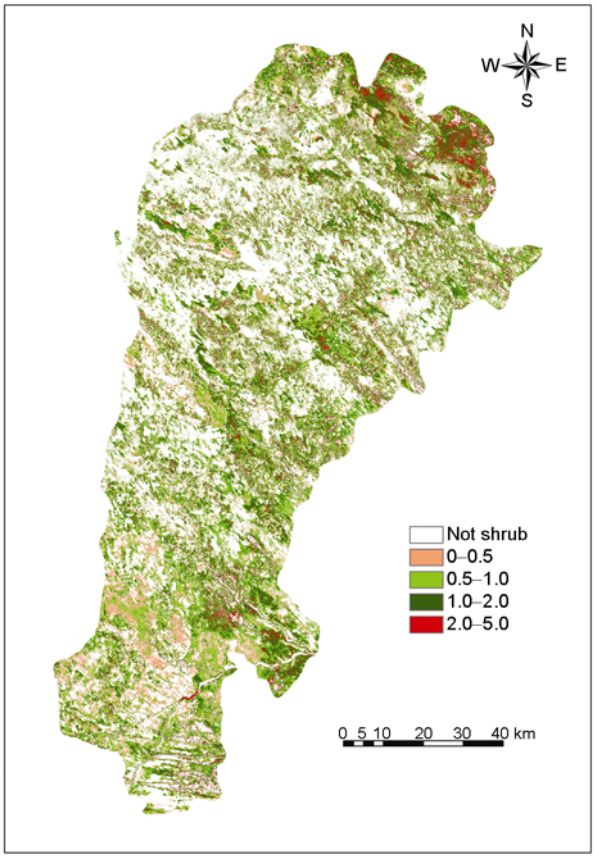

Figure 4 Map of the shrub *LAI* inversion result.

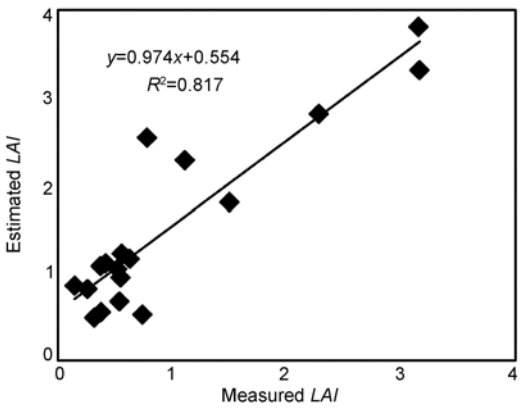

Figure 5 Relationship between ground-measured *LAI* and model-estimated *LAI*.

tion to one anomaly, there are 18 valid independent samples. The coefficient of determination R^2 is 0.817 for the *LAI* ($P < 0.0001$). The calculated root-mean-squared error for the *LAI* is 0.173. Most of the interpreted results of the *LAI* seem to equate with the field-measured values. Since most of the shrub species in sample plots of the study area are low shrubs, most of the measured *LAI* values are in the range 0–1, and the estimated *LAI*s appear to be higher than the measured values, which is probably due to branches, trunk and leaves not being effectively separated in the HJ-1B images. In some plots with high vegetation density, *LAI* values are high and the measured and estimated values are in good agreement. Therefore, the reliability of the model output is considered to be acceptable.

4 Conclusions and discussion

The inverted GO model combined with the spectral umixing analysis used in this study proved to be useful in deriving the shrub *LAI* from HJ-1 CCD data in Wushen Banner of Inner Mongolia in the Mu Us Sandland. The accuracy of the inverted model results mainly depends on the obtained *M*. Therefore, for a better calibration of the model, sensitivity analysis may be performed, estimating the sensitivity of *M* to the sunlit background fraction and the canopy shape parameters.

We evaluated the efficiency and usefulness of using HJ-1 CCD data in combination with a physical-based canopy reflectance model to determine the shrub *LAI* at regional scale. Even though the selected procedures will require further detailed analysis in the future, the presented results suggest confidence in the approach. Besides the shrub *LAI*, shrub structural and biophysical attributes, such as shrub height, crown closure, and biomass, might also be estimated more exactly through the inversion of canopy reflectance models with support of high-spatial-resolution and hyperspectral remote-sensing data. Consequently, quantitative monitoring of shrubland and its changes over time using effective and coherent models will be a major future goal.

This work was supported by National Natural Science Foundation of China (Grant No. 40871173), Special Grant for Prevention and Treatment of Infectious Diseases (Grant No. 2008ZX10004-012), and National State Basic Research Program of China (Grant No. 2007CB714404). The authors also wish to thank all those who assisted in this work.

1 Chen J M, Black T A. Defining leaf area index for non-flat leaves. Plant Cell Environ, 1992, 15: 421–429
2 Thenkabail P S, Enclona E A, Ashton M S, et al. Hyperion, IKONOS, ALI, and ETM+ sensors in the study of African rainforests. Remote Sens Environ, 2004, 90: 23–43
3 Franklin S E, Wulder M A, Gerylo G R. Texture analysis of IKONOS panchromatic data for Douglas-fir forest age class separability in British Columbia. Int J Remote Sens, 2001, 22: 2627–2632
4 Thenkabail P S, Hall J, Lin T, et al. Detecting floristic structure and pattern across topographic and moisture gradients in a mixed species Central African forest using IKONOS and Landsat-7 ETM+ images. Int J Appl Earth Obs, 2003, 4: 255–270
5 Zhang H, Jiao Z T, Yang H, et al. Research about scale effect of histogram. Sci China Ser D-Earth Sci, 2002, 45: 949–960
6 Chen X, Vierling L, Rowell E, et al. Using lidar and effective *LAI* data to evaluate IKONOS and Landsat 7 ETM+ vegetation cover estimates in a ponderosa pine forest. Remote Sens Environ, 2004, 91: 14–26
7 Bao Y F, Cao C X, Zhang H, et al. Synchronous estimation of DTM and fractional vegetation cover in forested area from airborne LiDAR height and intensity data. Sci China Ser E-Technol Sci, 2008,

51(Suppl): 176–187
8 Cao C X. Analysis of vegetation index (Band 4/Band 3) change and pine forest damage in the western part of Hiroshima Prefecture in 1987, 1992 and 1996 using satellite imagery. Proceedings of the 46th Japanese Conference on Ecological Research, 1999. 256
9 Colombo R, Bellingeri D, Fasolini D, et al. Retrieval of leaf area index in different vegetation types using high resolution satellite data. Remote Sens Environ, 2003, 86: 120–131
10 Sonnentag O, Chen J M, Roberts D A, et al. Mapping tree and shrub leaf area indices in an ombrotrophic peatland through multiple endmember spectral unmixing. Remote Sens Environ, 2007, 109: 342–360
11 Zhang N, Zhao Y S. Estimating leaf area index by inversion of reflectance model for semiarid natural grasslands. Sci China Ser D-Earth Sci, 2009, 52: 66–84
12 Chen J M, Li X, Nilson T, et al. Recent advances in geometrical optical modeling and its applications. Remote Sens Rev, 2000, 18: 227–262
13 Li X, Strahler A H. Geometric-optical bidirectional reflectance modeling of the discrete crown vegetation canopy: Effect of crown shape and mutual shadowing. IEEE Trans Geosci Remote, 1992, 30: 276–291
14 Ni W, Li X. A coupled vegetation-soil bidirectional reflectance model for a semi-arid landscape. Remote Sens Environ, 2000, 74: 113–124
15 Chopping M, Su L, Laliberte A, et al. Mapping shrub abundance in desert grasslands using geometric-optical modeling and multi-angle remote sensing with CHRIS/Proba. Remote Sens Environ, 2006, 104: 62–73
16 Gemmell F. Testing the utility of multi-angle spectral data for reducing the effects of background spectral variations in forest reflectance model inversion. Remote Sens Environ, 2000, 72: 46–63
17 Scarth P, Phinn S. Determining forest structural attributes using an inverted geometric-optical model in mixed eucalypt forests, Southeast Queensland, Australia. Remote Sens Environ, 2000, 71: 141–157
18 Chopping M J, Rango A, Havstad K M, et al. Canopy attributes of Chihuahuan Desert grassland and transition communities derived from multi-angular 0.65 μm airborne imagery. Remote Sens Environ, 2003, 85: 339–354
19 Chopping M, Su L, Rango A, et al. Modeling the reflectance anisotropy of Chihuahuan Desert grass-shrub transition canopy-soil complexes. Int J Remote Sens, 2004, 25: 2725–2745
20 Qin W, Gerstl S A W. 3-D scene modeling of Jornada semi-desert vegetation cover and its radiation regime. Remote Sens Environ, 2000, 74: 145–162
21 Bowyer P, Danson F M, Trodd N M, et al. Prospects for the remote sensing of savanna vegetation using physically based plant canopy reflectance models. Proceeding of Remote Sensing and Photogrammetry Society Annual General Meeting, 2001. 241–245
22 Gemmell F. Testing the utility of multi-angle spectral data for reducing the effects of background spectral variations in forest reflectance model inversion. Remote Sens Environ, 2000, 72: 46–63
23 Wang Q, Yang Y, Wu C Q. Study of retrieving models for chlorophyll-a concentration based on HJ-1A HIS image (in Chinese with English abstract). Spacecraft Eng, 2009, 18: 133–137
24 Yi L, Wang X, Liu B. Researches on HJ-1 satellite image quality and land use classification precision (in Chinese with English abstract). Remote Sens for Land Resour, 2009, 81: 74–77
25 Ya J, Zhu Z H, Dong J L. Study on the succession of vegetation after aerial seeding in Maowusu Sandy Land—Taking Wushen Banner of Inner Mongolia as all example. Inner Mongolia Forestr Invest Des, 2008, 31: 1–4
26 Richter R. Atmospheric correction of DAIS hyperspectral image data. Comput Geosci, 1996, 22: 785–793
27 Palluconi F, Hoover C, Alley R, et al. An atmospheric correction method for ASTER thermal radiometry over land. ASTER Standard Data Product, AST09, 1996
28 Strahler A H, Jupp D L B. Modeling bidirectional reflectance of forests and woodlands using boolean models and geometric optics. Remote Sens Environ, 1990, 34: 153–166
29 Lemeur R, Blad B L. A critical review of light models for estimating the shortwave radiation regime of plant canopies. Agr Meteorol, 1974, 14: 255–286